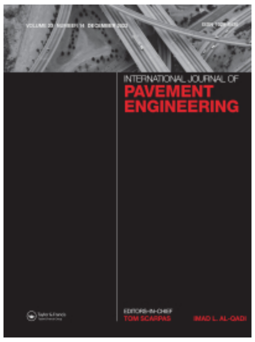

International Journal of Pavement Engineering

ISSN: (Print) (Online) Journal homepage: www.tandfonline.com/journals/gpav20

Flexural fatigue performance of a high-thixotropy UHPC

Anny Medicis, Hermes Vacca, Yezid Alvarado, Orlando Rincón & Daniel Ruiz

To cite this article: Anny Medicis, Hermes Vacca, Yezid Alvarado, Orlando Rincón & Daniel Ruiz (2023) Flexural fatigue performance of a high-thixotropy UHPC, International Journal of Pavement Engineering, 24:2, 2282004, DOI: 10.1080/10298436.2023.2282004

To link to this article: https://doi.org/10.1080/10298436.2023.2282004

Published online: 01 Dec 2023.

INTERNATIONAL JOURNAL OF PAVEMENT ENGINEERING
2023, VOL. 24, NO. 2, 2282004
https://doi.org/10.1080/10298436.2023.2282004

Taylor & Francis
Taylor & Francis Group

Flexural fatigue performance of a high-thixotropy UHPC

Anny Medicis, Hermes Vacca, Yezid Alvarado, Orlando Rincón and Daniel Ruiz

Department of Civil Engineering, School of Engineering, Pontificia Universidad Javeriana, Bogota, Colombia

ABSTRACT

This research aims to perform a comparison of the mechanical response and the fatigue behaviour of two Ultra-High Performance Concrete (UHPC) mixtures subjected to bending loads: a regular UHPC and a high-thixotropy UHPC. The same materials were used in both mixtures and the only difference was the proportions of water and additive. Rheological tests were performed to validate the thixotropy of mixtures in fresh-state. Additionally, image analysis was applied to get fibre distribution and orientation from beam-cut slices. Thus, the Image pixel complete colour structure (RGB) was analysed to avoid greyscale transformations because of its loss of information. Finally, three-point bending tests were conducted over pre-cracked beams to establish a fatigue equation for the mixtures. Experimental results showed that high-thixotropy UHPC has mechanical properties comparable to regular UHPC.

ARTICLE HISTORY
Received 21 April 2023
Accepted 6 November 2023

KEYWORDS
UHPC; flexural fatigue; rheology; thixotropy

1. Introduction

Ultra-high-performance concrete (UHPC) is a cementitious material characterised by a dense microstructure that generates ultra-high strength, ductility, and durability properties, compared to conventional concrete (Soliman and Tagnit-Hamou 2017, Chen *et al.* 2019, Li *et al.* 2020, Sohail *et al.* 2021). Some researchers have reported that the specified compressive strengths for UHPC are over 120 MPa (Abbas *et al.* 2015, Mishra and Singh 2019, Bajaber and Hakeem 2021), flexural strength over 15 MPa (Yoo *et al.* 2017, Huang *et al.* 2021, Li *et al.* 2021). Consequently, there are numerous applications of UHPC such as in bridge decks and components, nuclear power plants, shells and high-rise towers, repair and rehabilitation of infrastructural components, etc. Schmidt and Fehling (2005), Jiao *et al.* (2020), and Arora *et al.* (2019). Other studies have shown a wide range of applications of UHPC in road infrastructure (Habert *et al.* 2013, Azmee and Shafiq 2018, Meléndez *et al.* 2022, Helsel *et al.* 2023). However, properties such as yield stress, plastic viscosity, and thixotropy must be evaluated to guarantee an adequate performance in the casting processes in some elements or structures of UHPC (Khayat *et al.* 2019). For example, in the case of placing UHPC as a paving slab, it is necessary to modify the thixotropic behaviour of the UHPC, indispensably reducing the fluidity of the concrete to enable placement on inclined surfaces (Haber *et al.* 2018, Sritharan *et al.* 2018).

The Federal Highway Administration (FHWA) has investigated that the UHPC rheology must be evaluated for each of the working dosages, which seek to produce concrete with greater thixotropy and achieve the workability required for pavement application (Haber *et al.* 2017). Thixotropy of the cement-based materials is typically measured in terms of static yield stress and its variation with time (Omran *et al.* 2011). Concrete thixotropic behaviour is the reversible and time-dependent decreasing of viscosity, generated when a shear rate is applied during its fresh state during its casting process, and in the reverse process, when the shear rate effect is removed (Barnes 1997, Zhu *et al.* 2021). A thixotropic UHPC mixture may have yield stress sufficient to prevent the particles from settling (Roussel 2006). Besides, the thixotropy is dependent on the mix constituents (González-Taboada *et al.* 2018), thus, the inclusion of additives can significantly change the rheological properties and induce high yield stress and thixotropy of the concrete (Kolawole *et al.* 2019). Though, when the increased value of yield stress and plastic viscosity, mixtures often take on a high cohesion which may improve the ability to stabilise fibres but decrease the workability for pouring or placing; even this effect can influence the orientation and distribution of fibres (Wang *et al.* 2017).

It has been reported that the fibres in the concrete matrix provide a significant contribution to the mechanical properties of cementitious materials in the fresh and hardened state. The mechanical behaviour of fibre-reinforced concrete or composites is influenced by the fibre characteristics, such as shape, volume fraction, and orientation. Fibre aligning can simultaneously improve the cracking strength, ultimate strength and ductility of UHPC under flexure and tension. However, steel fibres are randomly dispersed in UHPC when being prepared by a direct cast method, decreasing the mechanical behaviour up to 70% for the aligned fibres (Swamy 1975, Martinie *et al.* 2010, Martinie and Roussel 2011, Kang and Kim 2012, Huang *et al.* 2018, Raju *et al.* 2020, Zhang *et al.* 2020). Figure 1 gives a schematic representation of the typical Stress-CMOD (crack mouth opening displacement) curve. As observed, the curve pattern has four phases: in I and II it is reported an elastic behaviour until it reaches its elastic limit strength, and the microcracks start to appear, leading to a sudden drop of stress at F_{lop} (Makita and Brühwiler

CONTACT Hermes Vacca vacca@javeriana.edu.co

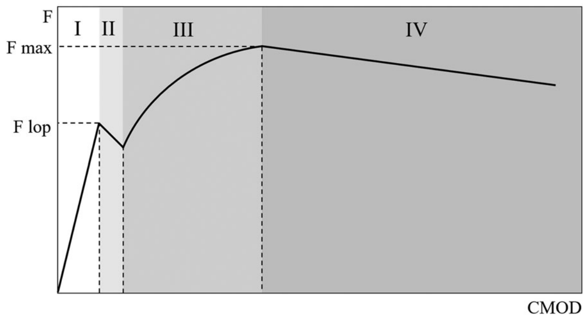

Figure 1. Schematic representation of flexural behaviour of steel fibre reinforced concrete.

2014), and, in III and IV, the microcracks are controlled by fibres leading to the increase of ultimate strength (F_{max}) and post-peak behaviour (Christidis *et al.* 2021).

On the other hand, despite the increasing interest in UHPC and its potential applications, to date, representative fatigue test results of UHPC have not been reported that could be used on specific models. Instead, most studies have focussed on evaluating its mechanical and durability performance due to the extraordinary strength characteristics (Bajaber and Hakeem 2021). However, any structure can suffer from cracks due to repeated loads during its service life; therefore, assessing flexural fatigue behaviour is important.

Most of the research reports that have studied the bending fatigue behaviour in steel fibre reinforced concrete (SFRC) have been carried out in pre-cracked beams, following the Crack Mouth Opening Displacement (CMOD) in the function of the applied loads, and found that the opening of the crack determines the fatigue life. For instance, the flexural fatigue performance of high-performance fibre-reinforced concrete (HPFRC) was reported (Naaman and Hammoud 1998). In this case, the beams were pre-cracked before the cyclic loading test, with two to three visible cracks. The specimens were subjected to the loading range sustained the 10%, 80%, and 90%. The researchers suggested an endurance limit of about 68% of the ultimate load for 5,000,000 cycles. Germano *et al.* (2016) examined the effects of fibre content (0.5 and 1%) on the flexural fatigue behaviour of plain and steel fibre reinforced concrete (SFRC). The fatigue tests were performed on pre-cracked notched specimens, and it was done considerating a drop of 5% of the referred beam peak load. Three fatigue load levels (64, 75, and 85%) were adapted with a constant amplitude (equal to 50% of load). The results showed that the crack opening increment per cycle and the crack opening range, are two parameters that govern the fatigue life of the concrete. Furthermore, the steel fibres improve the energy dissipation capacity of the concrete. González *et al.* (2018) evaluated the effect of fatigue loads on the residual tensile strength of steel fibre reinforced concretes. The maximum and minimum applied stress was 65% and 5% of its flexural strength, respectively. They showed that cyclic loads caused a progressive reduction of the stiffness of specimens. This effect was attributed to the cracking in the fibre-cement paste interface, causing a decrease in the fibre-concrete bond. Carlesso *et al.* (2019) researched a structural design-oriented analysis on the behaviour of pre-cracked beams subjected to flexural fatigue loading. Different load ranges were applied: 65, 70, 75, 80, 85, and 90% of the ultimate flexural capacity. The endurance limit was defined at 2,000,000 cycles, and it was reached at 66% of the flexural strength.

Given the above, it is important to evaluate the fatigue performance of pre-cracked concrete specimens. Therefore, this study focussed on evaluating the fatigue performance of pre-cracked samples subjected to bending. Two UHPC mixtures were studied, the first with high-thixotropy UHPC and a regular UHPC. For the purpose of characterise the mixtures, the experimental programme included rheological tests in the fresh state and compressive strength, modulus of rupture, modulus of elasticity, identification of fibre orientation and distribution, and, finally, fatigue in hardened conditions. The studied variables in the experimental programme were the maximum number of cycles reached (N) and the load level (S) in fatigue tests.

2. Experimental program

2.1. Material dosing

Two UHPC mixtures were manufactured in this study: the first was a self-compacting regular UHPC labelled as UHPC-A, and the second, was designed to be more thixotropic in the fresh state than UHPC-A and labelled as UHPC-T. The Thixotropy of the mixtures was modified, reducing the amount of additive. Both mixes were prepared with the same materials and only differed between them in the proportions of water and additive.

Materials and the mix proportions are presented in Table 1. The binder was composed of Portland cement, silica fume, and calcium carbonate; the fine aggregate had a particle size under 600 m. In addition, an superplasticizer additive SP (High Range water reducing, HRWR) agent based on polycarboxylic was used to save water (ASTM C494 requirements for Type F); and steel microfibres with 2% volume fraction (this percentage has been commonly used in prior studies (Zhang *et al.* 2020, Bajaber and Hakeem 2021, Shao *et al.* 2022), which had a length of 13 mm and diameter of 0.20 mm. The tensile strength and Young modulus of the fibres were 2750 MPa and 200 GPa, respectively.

The mixing and casting process followed the same procedure for both mixtures. The manufacturing of UHPC mixes was carried out in a planetary mixer with a capacity of 0.1 m^3. Mix preparation for each different dosing was carried out in an average time of 31 min (t_f). Subsequently, the characterisation tests were carried out in the fresh state (mini-slump and rheology). Finally, the samples were manufactured for the characterisation in the hardened state and fatigue. Table 2 shows the times of the mixing and casting process.

Table 1. Composition of mixtures.

Material	UHPC-A	UHPC-T
Portland Cement (kg/m^3)	740.0	740.0
Calcium carbonate (kg/m^3)	310.0	310.0
Silica fume (kg/m^3)	210.0	210.0
Siliceous Sand (kg/m^3)	802.2	802.2
Steel fibre (kg/m^3)	153.0	153.0
Water (kg/m^3)	219.0	220.7
Superplasticizer SP (kg/m^3)	24.7	22.5
SP/*b*	0.0196	0.0180

Table 2. Details of the mixing procedures, testing and sampling.

Step	Start time (mm:ss)	Finish time (mm:ss)	Description of action
1	00:00	01:00	Mix SP + Water
2 = (t_o)	00:00	00:30	Add 50% dry materials
3	00:30	01:30	Mix
4	01:30	02:00	Add 25% dry materials
5	02:00	08:00	Mix
6	08:00	08:30	Add 25% dry materials
7	08:30	27:00	Mix
8	27:00	27:30	Add fibre
9 = (t_f)	27:30	31:00	Mix
10	31:00	37:00	Mix
11	37:00	40:00	Test preparation
12	40:00	48:00	Simultaneous tests for characterisation in the fresh state
13	48:00	–	Preparation of specimens for hardened state

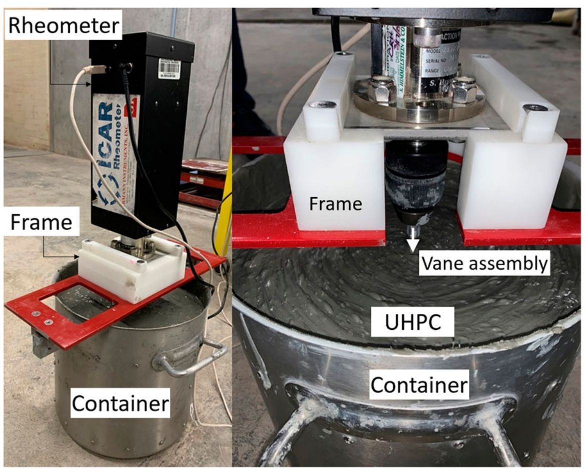

Figure 2. ICAR rheometer.

2.2. Characterisation in fresh state

The workability was estimated using mini-slump test (ASTM C1856). The rheological properties were measured using a ICAR rheometer as shown in Figure 2. It consist of a cylindrical container, an electrical motor and a four bladed vane which is positioned in the centre of the concrete mixture. The mixtures were repeated five times with the same dosage and in the same laboratory.

The stress growth procedure was used in this study to determine the static yield stress (τ_s). This parameter was determined with the torque as a function of time at a constant and very low rotational speed of 0.025 rps (Dzuy and Boger 1985, Schwartzentruber *et al.* 2006, Ahari *et al.* 2015). The Time-Torque graph (Figure 3) shows the elastic behaviour before reaching the curve's peak, in order to then have the material display a plastic behaviour. Therefore, the stress τ_s was calculated as follows (Equation (1)):

$$\tau_s = \frac{2T}{\pi D^3\left(\frac{h}{D}+\frac{1}{3}\right)} \quad (1)$$

Where, T is the maximum torque (Nm), D is the diameter of the vane (0.127 m) and H is the height of the vane (0.127 m).

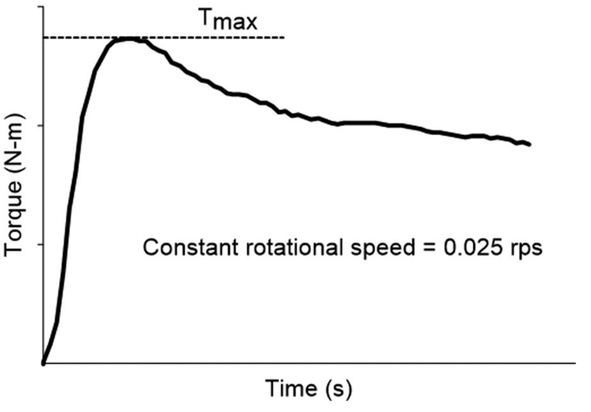

Figure 3. Maximum torque measurement method.

After stress growth or overcoming a particular value of yield stress τ_s the flow starts. Once the flow starts, stress τ and the shear $\dot{\gamma}$, shows the direct relationship. The slope of this flow curve defines the plastic viscosity which is generally denoted by μ_p. The flow behaviour of concrete according to the Bingham model is illustrated in Equation (2) (Jau and Yang 2010, Li *et al.* 2020, Nazar *et al.* 2020). Therefore, to determine the rheological parameters using the ICAR rheometer, the rotational speed in the rheometer was reduced from 0.5 to 0.025 rps in 7 steps (Pilar *et al.* 2021). The dynamic yield stress (τ_o) and viscosity (μ_p) in fundamental units can be obtained using the G values in Equation (3) from the Reiner-Riwlin transformation equations, as shown in Equation (4) and (5).

$$\tau = \tau_o + \mu_p \dot{\gamma} \quad (2)$$

$$T = G + H \cdot N \quad (3)$$

$$\tau_o = \frac{G}{4\pi h}\left(\frac{1}{R_1^2}-\frac{1}{R_2^2}\right) - \frac{1}{ln\left(\frac{R_2}{R_1}\right)} \quad (4)$$

$$\mu_p = \frac{H}{8\pi^2 h}\left(\frac{1}{R_1^2}-\frac{1}{R_2^2}\right) \quad (5)$$

Where T (Nm) is the torque; G (Nm) is the intercept of the flow curve; H (Nm/s) is the slope of the flow curve; N (m/s) is the rotational velocity; R_1 is the inner cylinder radius; R_2 is the outer cylinder radius of the container.

To measure thixotropy, the test process was divided into two stages. Firstly, the mixture was loaded at a shear rate from 0.05 rev/s to 0.5 rev/s. Immediately after that, the mixture was unloaded at a shear rate from 0.5 rev/s to 0.05 rev/s. The area between both curves reflects the thixotropy (Roussel 2006, Kolawole *et al.* 2019).

2.3. Manufacturing of test samples

Concrete was manually poured into the slabs molds (5 molds per mixture) using a bucket, following a casting method in a zigzag shape to propitiate a drag force to enhance the aligning of steel fibres in the beams (Raju *et al.* 2020, Zhang *et al.* 2020) (Figure 4(a)). Dimensions of Slab molds were 400 mm × 450 mm × 50 mm. The slabs were cut after curing

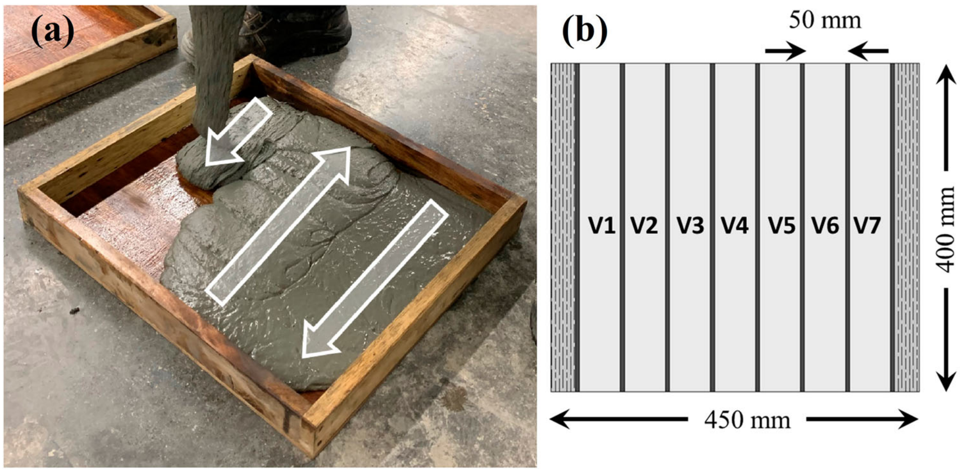

Figure 4. Process of pouring concrete into the slab (a), and slab cutting configuration (b).

for two days into 50 mm × 50 mm × 400 mm beams to obtain the specimens for bending and fatigue tests (Figure 4(b)). All specimens were cured for 56 days before being tested, to avoid a possible strength increase during the fatigue tests (Goel *et al.* 2012, Arora and Singh 2017).

2.4. Characterisation in hardened state

Compressive strength was measured according to standard ASTM C1856 and modulus of elasticity according to standard ASTM C469 by using a IBERTEST MEH-1500 universal testing machine, and five specimens were tested for each test. The three point bending tests were carried out according to Test Method EN 14651:2007 (British Standards Institution 2008) for beams notched in the centre of the lower face, using a MTS 311.41 servo-hydraulic test system. To record the CMOD, beams were instrumented with a clip gauge, as shown in Figure 5.

2.4.1. Distribution and orientation of fibres

To determine the distribution and orientation of the fibre, the same samples of the bending test were used after being tested. The analysis section corresponded to the transverse section of the beam where the failure occurred. Therefore, it does not include the distribution analysis along the slab, which can restrict free rotation, leading to a better orientation of the fibres located near to the formwork, as proposed by other authors Martinie and Roussel (2011). Images were acquired through commercial cameras with resolutions of 2 to 18 Megapixels, looking to get details about fibre-matrix interaction, reaching next to the microscale domain, to improve the fibre detection process at the pixel analysis level during image analysis. Image analysis can be understood as the conversion of an image into a number or set of numbers, in this case allowing the characteristics of a material to be identified (Heilbronner and Barrett 2013).

The images were taken in the laboratory, under controlled conditions of light, distance, distortion, and content of the samples in surface moisture. Thus, it was possible to characterise the colour structure of the samples and their constitutive elements (matrix, voids, and fibres) reducing potential biases and helping to develop an improved image segmentation methodology for fibre detection based on detailed colour changes. In contrast, conventional image analysis approaches developed using gray scale transformed images. This transformation process causes a loss of information in pixels near the fibre boundary; therefore, some recovered fibre shapes are imprecise affecting the frequency count. Hence, applying the stated methodology for image analysis by Rincon *et al.* (2016) through colorimetric descriptors and statistics from the image, an improved Image analysis algorithm was coded in Microsoft Visual Studio 2019 text registered for fibre detection. The algorithm was structured considering the relationship between UHPC sample surface features (matrix, voids, and fibres) and color changes at the pixel level, thus colour alterations on sample surface regarding matrix can come mainly in two ways: changes due to voids or fibres presence. First images from samples were studied in order to define the most relevant colour structure characteristics by analysing the variations for the R, G, B channels (Figure 6), looking for indicators that characterise each scene element, in order to make a better image segmentation. Nevertheless, different image descriptors and colorimetric indexes such as tone, brightness, and saturation indexes were tested seeking a better classification scheme for the algorithm (Figure 7) (Rincón and Ocampo 2017).

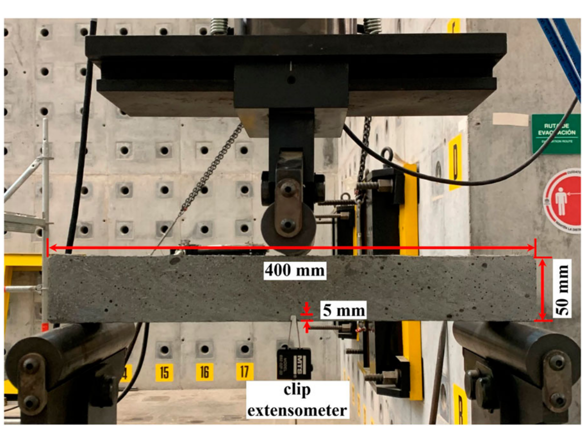

Figure 5. Three-point bending test set-up.

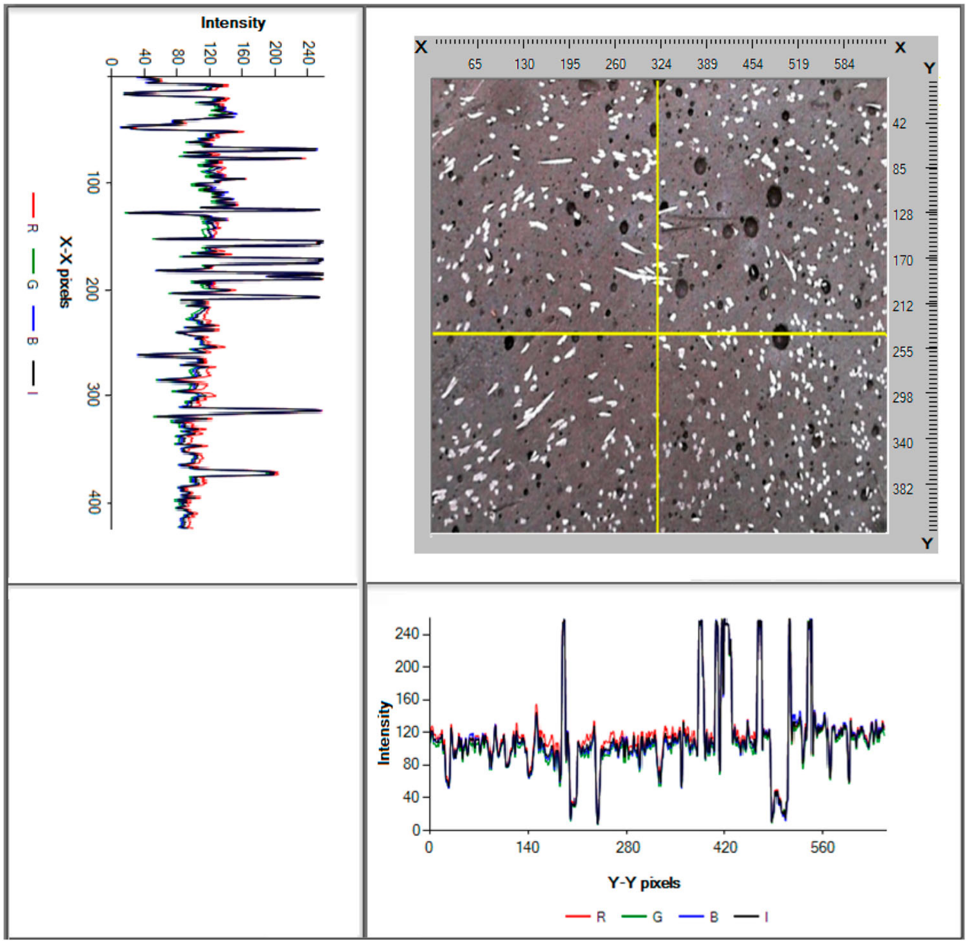

Figure 6. Detail of changes analysis for R, G, B Channels from VIS UHPC Image.

After obtaining the processed image, the number of fibres per unit area, n_f (number/mm^2) (Equation (6)), and the inclined angle of a single fibre to the cutting plane θ (Equation (7)) can be computed as:

$$n_f = \frac{N_f}{A} \tag{6}$$

$$\theta = \cos^{-1}\frac{d_f}{a} \tag{7}$$

where N_f is the total number of fibres, A is the counted area. On the other hand, d_f is the fibre diameter and a major axis length (Martinie *et al.* 2010, Martinie and Roussel 2011, Huang *et al.* 2018, 2020). The fibre orientation number (α_θ) is computed as (Equation (8)) (Abrishambaf *et al.* 2017, Huang *et al.* 2018):

$$\alpha_\theta = \frac{1}{N_f^T}\sum_{n=1}^{N_f^T}\cos\theta_n \tag{8}$$

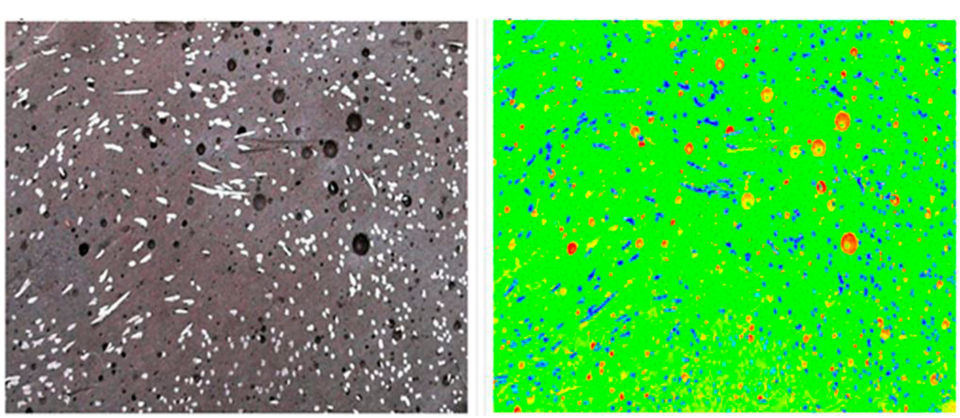

Figure 7. Example of classification of sample features applying colorimetric brightness index.

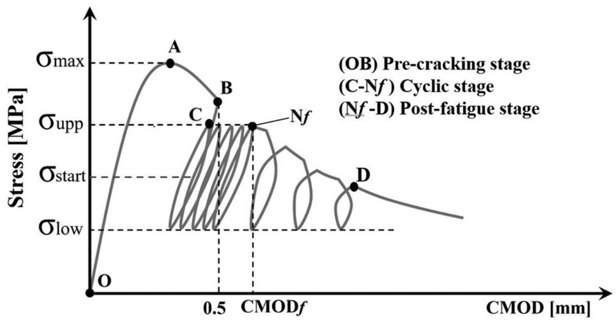

Figure 8. Schematic representation of the fatigue test.

where N_f^T is the total of fibre crossing the analysed section, θ_n is the inclined angle of the nth fibre.

2.5. Fatigue test

To determine for both analysed concrete, the flexural and fatigue performance, three-point bending tests were carried out on 17 specimens of UHPC-A and 20 of UHPC-T. In addition, strength contributed by the bonding of concrete and fibres was considered using a method that evaluates fatigue in pre-cracked samples. This method has been studied by several authors Naaman and Hammoud (1998), Carlesso *et al.* (2019), Germano *et al.* (2016), and González *et al.* (2018), among others. They studied fatigue response in pre-cracked FRC at a controlled load as a function of the CMOD.

Figure 8 shows the load history of each test. Tests start with a pre-cracking stage in which a monotonic load was applied at a constant rate of 0.05 mm/min, until obtaining a CMOD equal to 0.5 mm (acceptable service limit according to fib Model Code 2010 (MC2010, F. 2013, Carlesso *et al.* 2019). In this stage, maximum stress was obtained (Figure 8, point A). The upper and lower load limits for the fatigue cycle were calculated as shown below. Load upper limit (σ_{upp}) corresponds to a certain percentage of $\sigma_{\max}$ reaching a static zone in the test (Figure 8, point A). The lower limit (σ_{low}) is defined as ($\sigma_{low} = \sigma_{upp} - 0.5\sigma_{\max}$) (Germano *et al.* 2016). The stress at which cycles were started (σ_{start}) corresponded to the average of σ_{upp} and σ_{low} ($\sigma_{start} = (\sigma_{upp} + \sigma_{low})/2$).

Immediately after pre-cracking, load cycles were applied following a sinusoidal function at a frequency of 10 Hz until failure (Figure 8 point C). The test method used in this research differed from methods applied by the cited authors in σ_{upp} calculation; for cited authors, point a σ_{upp} was calculated based on the load corresponding to a CMOD equal to 0.5 mm ($\sigma_{0.5}$) (Figure 8 point B), while, for the purposes of this research, it was calculated based on $\sigma_{\max}$ value (Figure 8 point A), which corresponds to the maximum load reached during the pre-cracking zone. This change was adopted to evaluate the material's maximum capacity under the most critical conditions.

3. Results and discussion

3.1. Fresh state

The spreading diameters for UHPC-A and UHPC-T obtained through the mini slump were 240 ± 10 mm and 175 ± 8 mm, respectively (Figure 9). In the same way, the static yield stress values obtained were 59.9 ± 5.7 Pa for the UHPC-A mixture and 161.3 ± 10.3 Pa for UHPC-T.

The rheological parameters were calculated by fitting the flow curve using the Bingham Model, which has been used to describe the behaviour of this family of concretes (Feys *et al.* 2008, Güneyisi *et al.* 2016, Kolawole *et al.* 2019). Parameters were obtained by applying Equation (9), and are shown in Figure 10, where τ is shear stress (Pa), τ_0 is yield stress (Pa), μ is plastic viscosity (Pa s), γ is shear rate (1/s).

A reduction of approximately 8% of SP led to a decrease in workability and yield stress, increasing the thixotropy. Numerous researches have evaluated the effect of the variation of superplasticizer additives dosage on the thixotropy of mixture concretes. Qian *et al.* (2018) evaluated the thixotropy of cement paste by the variation of superplasticizer (SP) dosage. They found that the breakdown areas of thixotropy and the

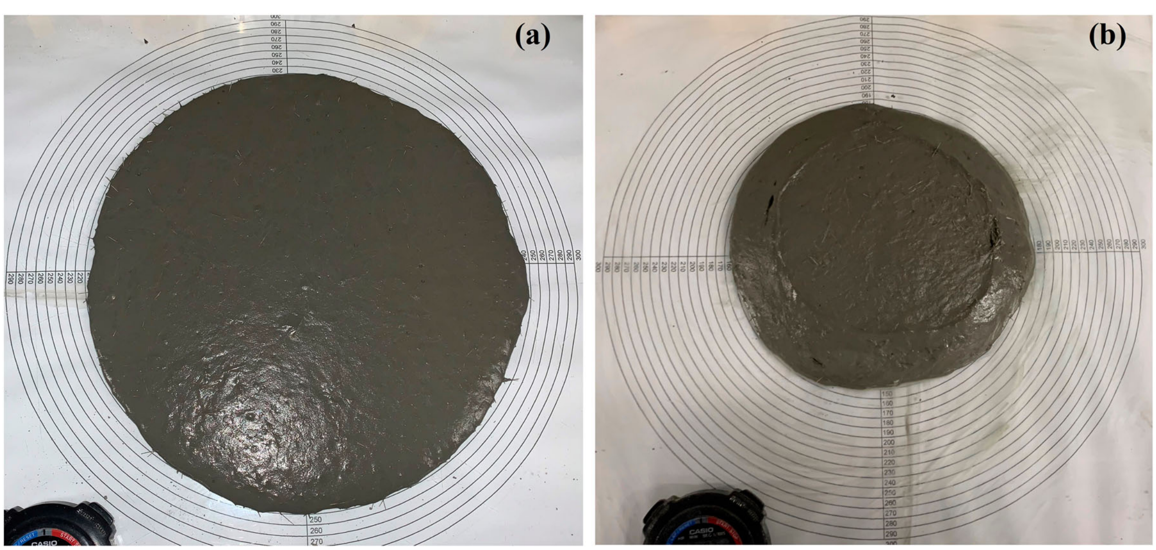

Figure 9. Spreading diameter of UHPC-A (a) and UHPC-T (b).

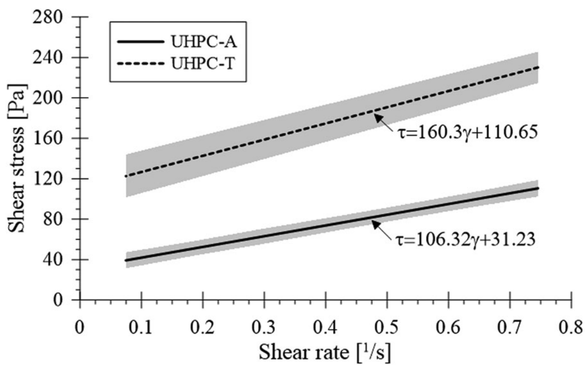

Figure 10. Rheological parameters according to the Bingham Model for UHPC-A and UHPC-T.

rheology parameter were affected by a change of SP. Lowke (2018) found that the thixotropic properties can be controlled by adjusting the water/binder ratio and additions. This can be explained by the attraction and separation of the particles. This is determined by the coverage of particle surfaces with adsorbed superplasticizer molecules. Lower surface coverage means a higher attractive force and thus a smaller bridging distance leading to an increase in thixotropic structure formation and decreasing workability.

$$\tau = \mu\gamma + \tau_0 \tag{9}$$

A comparison of the rheological parameters obtained in this research with a compilation of results from other authors Khayat *et al.* (2019) is shown in Table 3. The fluency stress of UHPC-A is within the range of a self-compacting concrete (SCC), and simultaneously, its plastic viscosity corresponds to that for UHPC. On the other hand, it was evidenced that UHPC-T presented more significant fluency stress than UHPC and SCC, demonstrating the rheological modification of the material due to changes made in the mix dosing.

Figure 11 presents the test cycles according to the Bingham Model for both mixtures. A significant change in the thixotropy can be seen. The shaded zones represent the thixotropy of each material and are enclosed by an increasing line (upper line of each mixture) and a decreasing line (lower line of each mix. It is evidenced that UHPC-T displays a significantly greater area (109.27 Pa/s), which demonstrates its thixotropic quality. On the other hand, UHPC-A shows a low thixotropy value (22.71 Pa/s), which is associated with its self-compacting behaviour.

Table 3. Typical rheological parameters for different concrete mixtures.

	Rheological parameter	
Concrete class	Yield stress (Pa)	Plastic viscosity (Pa.s)
CC[a]	500–2000	50–100
SCC[b]	5–50	100–400
HPC[c]	50–2000	50–550
UHPC[d]	10–100	20–200
UHPC-A	31.23	106.32
UHPC-T	110.65	160.30

Notes:[a]Conventional Concrete (Marković 2006).[b]Self-Compacting Concrete (Mardani-Aghabaglou *et al.* 2013).[c]High Performance Concrete (Hu and de Larrard 1996).[d]Ultra High Performance Concrete (Choi *et al.* 2016, Meng and Khayat 2017).

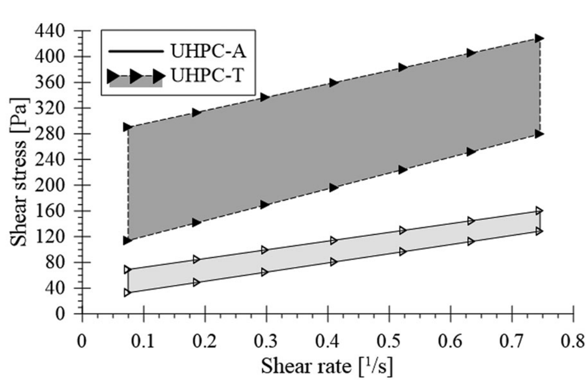

Figure 11. Rheological parameters according to the Bingham Model for UHPC-A and UHPC-T.

3.2. Hardened state

Mechanical properties are shown in Table 4. UHPC-A had a greater modulus of elasticity and greater compressive strength than UHPC-T. This can be attributed to the inversely proportional relation existing between compressive strength and the entrapped air in mixtures (Sanjayan *et al.* 2021). Dils *et al.* (2013) evaluated the influence of different cement types on the rheology and mechanical properties of UHPC. It was found that a 37% reduction of workability leads to an increase in the amount of entrapped air in the mixture and reduces its compressive strength by 27%. In this study, the workability of the UHPC-T was by approximately 27%, and the compressive strength was decreased by 13%.

The addition of fibres influences the entrapped air content in the mixture, the internal force between fibres and concrete, or between themselves (Yu *et al.* 2014). Therefore, despite the fact that mixtures were vibrated, there was a remaining portion of air entrapped in concrete, which in UHPC-A was smaller due to its self-compacting feature. At the same time, due to the high viscosity and fluency stress of UHPC-T, this mixture had a greater entrapped air content, which in the hardened state means more pores.

3.2.1. Distribution and orientation of fibres

Table 5 presents the average results of the total fibres (N_f^T), the distribution (n_f), and the orientation factor (α_θ) in the analysed section for the mixtures of UHPC-A and UHPC-T. As expected, the values obtained for both study mixtures, in terms of the number of fibres and the distribution parameter with the proposed methodology, were consistent with those reported in other investigations for similar volumes of fibres

Table 4. Results of the characterisation tests in the hardened state of UHPFRC-A and UHPFRC-T.

Mixture	Test	Mean	CV (%)
UHPC-A	Compressive strength	146.46 MPa	9.17
	Elastic modulus	60.06 GPa	2.48
	Flexural strength σ_{lop}	12.60 MPa	5.72
	Flexural strength σ_{mor}	13.82 MPa	8.77
UHPC-T	Compressive strength	126.76 MPa	12.64
	Elastic modulus	56.10 GPa	2.07
	Flexural strength σ_{lop}	12.61 MPa	8.91
	Flexural strength σ_{mor}	22.08 MPa	3.86

Table 5. Results of the total fibres (N_f^T), distribution (n_f) and, orientation factor in the analysed section for UHPC-A and UHPC-T mixtures.

Mixture	N_f^T	n_f (fibre/mm^2)	CV (%)	α_θ	CV (%)
UHPC-A	1227	0.47	6.09	0.19	11.47
UHPC-T	1591	0.60	8.85	0.07	47.10

(Abrishambaf *et al.* 2017, Zhou and Uchida 2017, Huang *et al.* 2020). However, an increase in fibre distribution was identified in the UHPC-T mix compared to the self-compacting mix. This is attributed to the fact that the UHPC-A mixture has greater fluidity and the fibre can flow more freely with respect to the thixotropic mixture, even knowing that the method of pouring the mixture is favourable to the distribution of the fibre (Kang *et al.* 2011, Kang and Kim 2012, Huang *et al.* 2021).

The average flexural strength results are presented in Table 4. Fibre distribution for each individual specimen is shown in Figure 12; related to the flexural strength *lop* (limit of proportionality) in Figure 12(a); and flexural strength *mor* (modulus of rupture) in Figure 12(b). It was observed that the number of fibres per area unit (n_f) considerably affects the ultimate flexural strength σ_{mor}, while it hardly affects the first cracking strength σ_{lop}, as has been reported (Kang and Kim 2012). Therefore, the performance of the concrete matrix is responsible for the early strength results in UHPC.

A similar case was presented regarding the fibre orientation factor (α_θ) (Figure 13). The initial cracking stress (σ_{lop}) is stable with respect to the ultimate stress (σ_{mor}) (Figure 13 (a)), which validates the contribution to the mechanical behaviour of the UHPC matrix. On the other hand, according to Figure 13(b), an increase in σ_{mor} was observed for the UHPC-T mixture that is related to the lower values (close to zero) of the orientation factor. The last fact suggests that the orientation is favorable for the bending behaviour and ensures a greater ability of the fibres to control cracks, increasing the bending and tensile mechanical properties of the UHPC samples (Huang *et al.* 2021).

3.3. Fatigue test

Fatiga life was evaluated through the S-N curve. Fatigue tests comprised three stages, a pre-cracking stage (static), cyclic stage, and post-fatigue stage.

3.3.1. Cracking stage

In order to study the overall results, the median values of the static flexural strength were obtained by considering the results from the cracking stage of the fatigue test. The flexural median stress-CMOD curves of UHPC-A (a) and UHPC-T (b) are presented in Figure 14, and Table 6 shows the median characteristic stress values and the coefficient of variation. After the σ_{lop}, when the first matrix crack occurs and the fibres are activated, the UHPC-A presented a drop in the flexural strength, and then the strength increases surpassing the cracking load. On the other hand, the UHPC-T did not show this behaviour,

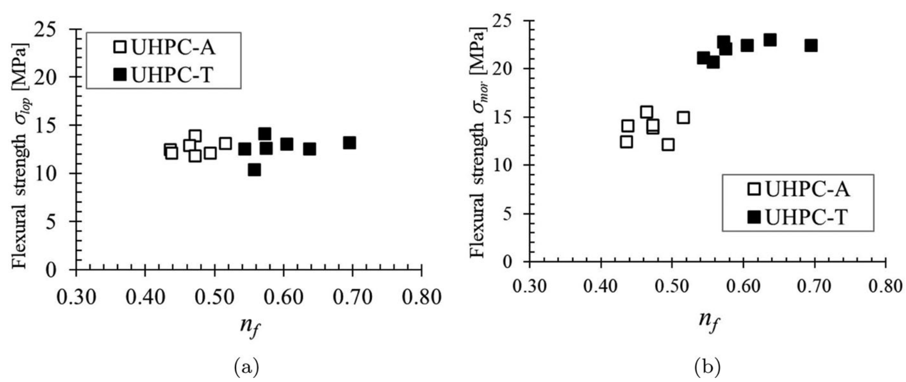

Figure 12. fibre distribution with respect to the flexural behaviour of UHPC mixtures. (a) Relation between fibre distribution n_f and σ_{lop} and (b) Relation between fibre distribution n_f and σ_{mor}.

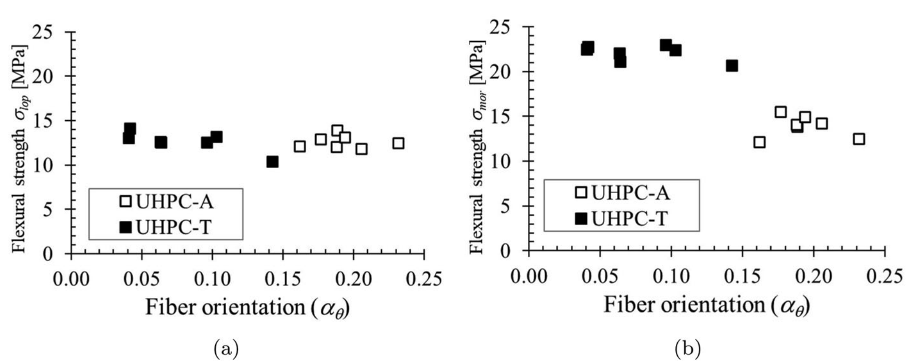

Figure 13. fibre orientation with respect to the flexural behaviour of UHPC mixtures. (a) Relation between orientation factor α_θ and σ_{lop} and (b) Relation between the orientation factor α_θ and the σ_{mor}.

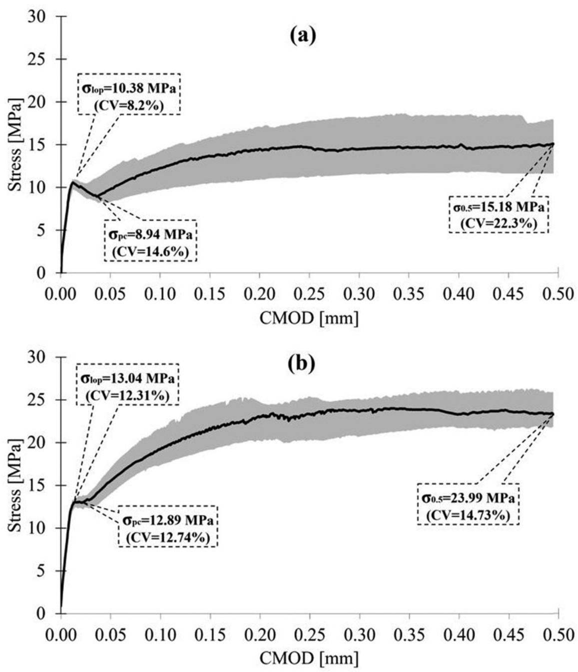

Figure 14. Median curve of pre-cracking process for UHPC-A (a) and UHPC-T (b).

Table 6. Results of bending tests of UHPC-A and UHPC-T expressed in mean and variation coefficient (CV).

Mixture	Test	Value	CV (%)
UHPC-A	σ_{lop}	10.38 MPa	8.20
	σ_{pc}	8.94 MPa	14.62
	0.5	15.18 MPa	22.30
UHPC-T	σ_{lop}	13.04 MPa	12.31
	σ_{pc}	12.89 MPa	12.74
	$\sigma_{0.5}$	23.99 MPa	14.73

after the σ_{lop}, it presented a discontinuity of the static flexural strength curve, and then the strength increases. Furthermore, comparison of the average shape curves shows higher coefficients of variation for UHPC-A.

The flexural strength and energy dissipated (area inside the curve) are higher in UHPC-T, which indicates that increasing the viscosity tended to improve the alignment parallel to the longitudinal direction of casting. Likewise, in prior studies, it has been reported that the orientation and distribution of steel fibres are affected by yield stress and rheology of fresh concrete, as verified in the previous sections of this study and other authors Meng and Khayat (2017) and Zhang *et al.* (2020).

3.3.2. Cyclic stage

The fatigue was evaluated based on the number of cycles endured until failure. Results are presented on Table 7, for UHPC-A and UHPC-T mixtures. It is commonly accepted that the failure occurred when σ_{upp} dropped 2%, and it was attributed to the sudden fibre pull-out (Germano *et al.* 2016).

The ratio between the σ_{upp} and the σ_{max} ($S = \sigma_{upp}/\sigma_{max}$) is plotted versus the logarithm of the number of cycles at failure ($LogN_f$) in Figure 15. It is noteworthy to mention that σ_{max} of UHPC-T was 58% higher than UHPC-A (it was discussed in Section 3.3.1), and therefore, for any level of stress, the

Table 7. Results from fatigue tests on UHPC-A and UHPC-T specimens tested.

UHPC-A		UHPC-T	
S	N_f	S	N_f
0.72	2,000,000	0.71	1,864,241
0.73	2,000,000	0.73	339,659
0.75	278,797	0.76	64,206
0.76	302,121	0.77	607,685
0.77	336,172	0.81	9688
0.79	133,349	0.83	3250
0.79	439,869	0.83	53,662
0.80	481,899	0.84	141,405
0.83	161,255	0.84	56,180
0.84	285,805	0.85	88,954
0.85	134,057	0.85	64,206
0.86	14,258	0.86	966
0.89	4779	0.87	22,732
0.89	350	0.88	721
0.91	6999	0.89	190
0.94	196	0.91	59
0.95	74	0.92	264
		0.94	126
		0.95	20
		0.98	66

performance of UHPC-T is higher than UHPC-A, e.g. at $S =$ 0.9, σ_{upp} of UHPC-A is 13.66 MPa ($N_f = 1514$ cycles), while σ_{upp} of UHPC-T would be 21.59 MPa ($N_f = 452$ cycles). However, at $\sigma_{upp} = 13.66$ MPa, UHPC-T would exhibit a fatigue endurance limit.

Fatigue damage was evidenced with the subcritical growth evidenced as a gradual decrease of σ_{upp} (Figure 8 (points C-D), which was interpreted as a sudden loss of adherence in the fibres and the impossibility of adjusting the level of applied stress due to the high frequency of the test. The reduction of load in fatigue tests may be related to the subcritical growth of CMOD, which led to failure. (Figure 8 (point C). Additionally, to ensure that all the load cycles within the fatigue test reached the same σ_{upp}, it was established that failure occurred when a reduction of 2% took place in σ_{upp} (Figure 8 (point C)).

The equations obtained with the linear regression of the S-N curve can predict the fatigue life of pre-cracked specimens. Fatigue performance of UHPC-A is superior at higher S levels; however, the fatigue line presents a lower slope, which can be interpreted as a reduction in the capacity to support load cycles compared to UHPC-T.

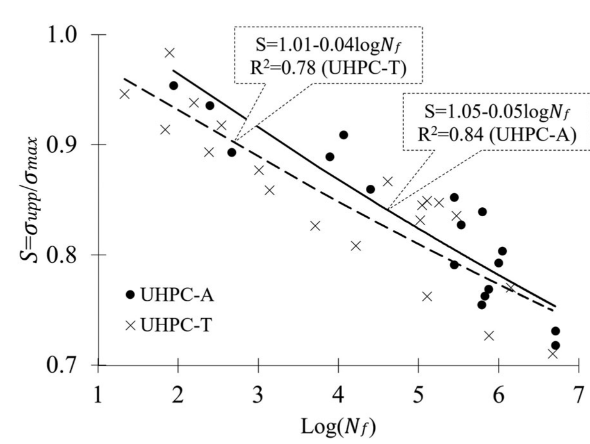

Figure 15. S-N line of UHPC-A and UHPC-T.

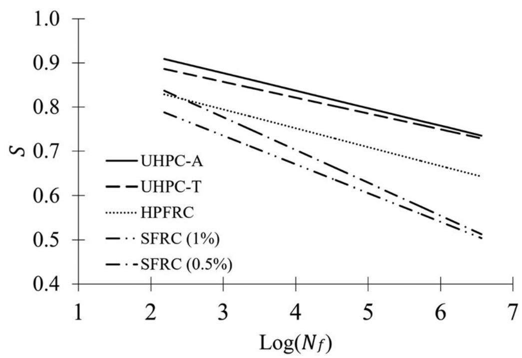

Figure 16. S-N line of UHPC-A, UHPC-T, HPFRC (Carlesso *et al.* 2019) and SFRC (Germano *et al.* 2016).

Figure 16 presents a comparison of fatigue lines for UHPC-A and UHPC-T mixtures, with studies of other authors that evaluated fatigue performance of special concretes using the same test method. The compared mixtures are a steel fibre-reinforced high-performance concrete (HPFRC Carlesso *et al.* 2019), and two SFRC (Germano *et al.* 2016). Likewise, a lower slope was observed in UHPC mixtures, interpreted as better fatigue performance. HPFRC had a similar slope to UHPC-A; however, it displayed lower S levels.

4. Conclusions

In this study, the flexural fatigue performance of a high-thixotropy UHPC was investigated. For this purpose, a three-point flexural and fatigue test with the notched was carried out for two types of UHPC mixtures, self-levelling and high-thixotropy. The fresh and hardened state characterisations of each mixture were analysed in order to identify the impact that rheology, distribution, and orientation had on mechanical performance. Based on the above results and discussion, the following conclusions can be made:

The reduction of the dose of superplasticizer in UHPC-T (8%) in the study mixture caused a decrease in the fluidity of 27% and an increase in both the elastic limit and the plastic viscosity of 354% and 150%, respectively. This evidences the increase in the thixotropy of the concrete as reported by other researchers.

The experimental results of this study and other research showed that changing the rheological properties could modify the fibre distribution and orientation. In this study, the change in rheological properties improved the flexural performance of UHPC, indicating that a 27% increase in fibre distribution caused by the decrease in superplasticizer contributed to the increase in maximum flexural strength in the samples test. However, decreasing the flowability of UHPC-T reduced the compressive strength by 15% and the modulus of elasticity by 7%.

Both UHPC-A and UHPC-T, at a load level (S) lower than 0.7, can resist more than 2,000,000 cycles, even when cracks are visible. This is possible since the mechanism of bonding between fibres and concrete stops and retains the crack's growth and development. In addition, comparing fatigue lines, UHPC-T presents a lower slope, which can be interpreted as a higher ability to endure load cycles than UHPC-A. In addition, for any stress level, the performance of UHPC-T would be higher than UHPC-A.

Acknowledgments

The research was developed by the Pontificia Universidad Javeriana and Cementos Argos S.A, that contributed with laboratory resources and time of professors and researchers. Also the authors of this work acknowledge and thank the support of the Civil Engineering Laboratory of Pontificia Universidad Javeriana and all technical staff, where the tests were carried out.

Disclosure statement

No potential conflict of interest was reported by the author(s).

Funding

This work was funded by Fondo Nacional de Financiamiento para la Ciencia, la Tecnología y la Innovación Francisco José de Caldas de Min-Ciencias, Republic of Colombia: Project Code 120380863881 Id: 63881, Rehabilitación de pavimentos con sobrecarpetas de concretos de Ultra Alto desempeño reforzado con fibras de acero UHPFRC. This research was developed by Pontificia Universidad Javeriana, and Argos company which contributed with laboratory resources and time of professors and researchers.

References

Abbas, S., Soliman, A.M., and Nehdi, M.L., 2015. Exploring mechanical and durability properties of ultra-high performance concrete incorporating various steel fiber lengths and dosages. *Construction and Building Materials*, 75, 429–441.

Abrishambaf, A., Pimentel, M., and Nunes, S., 2017. Influence of fibre orientation on the tensile behaviour of ultra-high performance fibre reinforced cementitious composites. *Cement and Concrete Research*, 97, 28–40.

Ahari, R.S., Erdem, T.K., and Ramyar, K., 2015. Thixotropy and structural breakdown properties of self consolidating concrete containing various supplementary cementitious materials. *Cement and Concrete Composites*, 59, 26–37.

Arora, A., et al., 2019. Fundamental insights into the compressive and flexural response of binder-and aggregate-optimized ultra-high performance concrete (UHPC). *Cement and Concrete Composites*, 98, 1–13.

Arora, S., and Singh, S.P., 2017. Fatigue strength and failure probability of concrete made with RCA. *Magazine of Concrete Research*, 69 (2), 55–67.

Azmee, N.M., and Shafiq, N., 2018. Ultra-high performance concrete: From fundamental to applications. *Case Studies in Construction Materials*, 9, e00197.

Bajaber, M., and Hakeem, I., 2021. UHPC evolution, development, and utilization in construction: A review. *Journal of Materials Research and Technology*, 10, 1058–1074.

Barnes, H.A., 1997. Thixotropy–a review. *Journal of Non-Newtonian Fluid Mechanics*, 70 (1-2), 1–33.

British Standards Institution., 2008. *Test method for metallic fibre concrete: measuring the flexural tensile strength (limit of proportionality (LOP), residual)*. BSI.

Carlesso, D.M., De la Fuente, A., and Cavalaro, S.H.P., 2019. Fatigue of cracked high performance fiber reinforced concrete subjected to bending. *Construction and Building Materials*, 220, 444–455.

Chen, J.J., Chen, H.N., and Li, G., 2019. Packing density improvement for improving strength of cement paste. *In*: *Materials science forum*. Vol. 943, 124–128.

Choi, M.S., et al., 2016. Estimation of rheological properties of UHPC using mini slump test. *Construction and Building Materials*, 106, 632–639.

Christidis, K., Badogiannis, E., and Mintzoli, C., 2021. Flexural behaviour of pumice lightweight concrete reinforced with end-hooked steel fibres. *In*: *Structures*. Vol. 33, 3835–3847.

Dils, J., Boel, V., and De Schutter, G., 2013. Influence of cement type and mixing pressure on air content, rheology and mechanical properties of UHPC. *Construction and Building Materials*, 41, 455–463.

Dzuy, N.Q., and Boger, D.V., 1985. Direct yield stress measurement with the vane method. *Journal of Rheology*, 29 (3), 335–347.

Feys, D., Verhoeven, R., and De Schutter, G., 2008. Fresh self compacting concrete, a shear thickening material. *Cement and Concrete Research*, 38 (7), 920–929.

Germano, F., Tiberti, G., and Plizzari, G., 2016. Post-peak fatigue performance of steel fiber reinforced concrete under flexure. *Materials and Structures*, 49, 4229–4245.

Goel, S., Singh, S., and Singh, P., 2012. Flexural fatigue strength and failure probability of self compacting fibre reinforced concrete beams. *Engineering Structures*, 40, 131–140.

González-Taboada, I., et al., 2018. Thixotropy and interlayer bond strength of self-compacting recycled concrete. *Construction and Building Materials*, 161, 479–488.

González, D.C., et al., 2018. Postcracking residual strengths of fiber-reinforced high-performance concrete after cyclic loading. *Structural Concrete*, 19 (2), 340–351.

Güneyisi, E., et al., 2016. Evaluation of the rheological behavior of fresh self-compacting rubberized concrete by using the Herschel-Bulkley and modified Bingham models. *Archives of Cvil and Mechanical Engineering*, 16, 9–19.

Haber, Z.B., et al., 2018. Bond characterization of UHPC overlays for concrete bridge decks: Laboratory and field testing. *Construction and Building Materials*, 190, 1056–1068.

Haber, Z.B., Munoz, J.F., and Graybeal, B.A., 2017. *Field testing of an ultra-high performance concrete overlay* (Tech. Rep.). United States. Federal Highway Administration. Office of Infrastructure ….

Habert, G., et al., 2013. Lowering the global warming impact of bridge rehabilitations by using Ultra High Performance Fibre Reinforced Concretes. *Cement and Concrete Composites*, 38, 1–11.

Heilbronner, R., and Barrett, S., 2013. *Image analysis in earth sciences: microstructures and textures of earth materials*. Vol. 129. Springer Science & Business Media.

Helsel, M.A., et al., 2023. Effect of bridge deck surface preparation on the consolidation and bond of UHPC overlays. *Construction and Building Materials*, 364, 129860.

Hu, C., and de Larrard, F., 1996. The rheology of fresh high-performance concrete. *Cement and Concrete Research*, 26 (2), 283–294.

Huang, H., et al., 2018. Improvement effect of steel fiber orientation control on mechanical performance of UHPC. *Construction and Building Materials*, 188, 709–721.

Huang, H., et al., 2020. SPH simulation and experimental investigation of fiber orientation in UHPC beams with different placements. *Construction and Building Materials*, 233, 117372.

Huang, H., et al., 2021. Influence of fiber alignment and length on flexural properties of UHPC. *Construction and Building Materials*, 290, 122863.

Huang, H., Gao, X., and Teng, L., 2021. Fiber alignment and its effect on mechanical properties of UHPC: An overview. *Construction and Building Materials*, 296, 123741.

Jau, W.C., and Yang, C.T., 2010. Development of a modified concrete rheometer to measure the rheological behavior of conventional and self-consolidating concretes. *Cement and Concrete Composites*, 32 (6), 450–460.

Jiao, Y., et al., 2020. Mechanical and fracture properties of ultra-high performance concrete (UHPC) containing waste glass sand as partial replacement material. *Journal of Cleaner Production*, 277, 123501.

Kang, S.T., et al., 2011. The effect of fibre distribution characteristics on the flexural strength of steel fibre-reinforced ultra high strength concrete. *Construction and Building Materials*, 25 (5), 2450–2457.

Kang, S.T., and Kim, J.K., 2012. Investigation on the flexural behavior of UHPCC considering the effect of fiber orientation distribution. *Construction and Building Materials*, 28 (1), 57–65.

Khayat, K.H., et al., 2019. Rheological properties of ultra-high-performance concrete–an overview. *Cement and Concrete Research*, 124, 105828.

Kolawole, J.T., Combrinck, R., and Boshoff, W.P., 2019. Measuring the thixotropy of conventional concrete: The influence of viscosity modifying agent, superplasticiser and water. *Construction and Building Materials*, 225, 853–867.

Li, J., et al., 2020. Durability of ultra-high performance concrete–A review. *Construction and Building Materials*, 255, 119296.

Li, H., et al., 2020. Investigations of mixing technique on the rheological properties of self-compacting concrete. *Applied Sciences*, 10 (15), 5189.

Li, S., et al., 2021. Influence of micromechanical property on the rate-dependent flexural strength of ultra-high performance concrete containing coarse aggregates (UHPC-CA). *Composites Part B: Engineering*, 227, 109394.

Lowke, D., 2018. Thixotropy of SCC–A model describing the effect of particle packing and superplasticizer adsorption on thixotropic structural build-up of the mortar phase based on interparticle interactions. *Cement and Concrete Research*, 104, 94–104.

Makita, T., and Brühwiler, E., 2014. Tensile fatigue behaviour of ultra-high performance fibre reinforced concrete (UHPFRC). *Materials and Structures*, 47, 475–491.

Mardani-Aghabaglou, A., et al., 2013. Effect of different types of superplasticizer on fresh, rheological and strength properties of self-consolidating concrete. *Construction and Building Materials*, 47, 1020–1025.

Marković, I., 2006. *High-performance hybrid-fibre concrete: Development and utilisation*. Doctorial Thesis, Universiteit van Belgrado, Servi, DUP Science, The Netherlands, 90–92.

Martinie, L., Rossi, P., and Roussel, N., 2010. Rheology of fiber reinforced cementitious materials: classification and prediction. *Cement and Concrete Research*, 40 (2), 226–234.

Martinie, L., and Roussel, N., 2011. Simple tools for fiber orientation prediction in industrial practice. *Cement and Concrete Research*, 41 (10), 993–1000.

MC2010, F., 2013. CEB-FIB model code for concrete structures 2010. *Lausanne: International Federation for Structural Concrete*.

Meléndez, A., et al., 2022. Comportamiento mecánico de una estructura de pavimento flexible rehabilitada con una sobrecapa de UHPFRC. *Revista ingeniería de construcción*, 37 (3), 335–344.

Meng, W., and Khayat, K.H., 2017. Improving flexural performance of ultra-high-performance concrete by rheology control of suspending mortar. *Composites Part B: Engineering*, 117, 26–34.

Mishra, O., and Singh, S., 2019. An overview of microstructural and material properties of ultra-high-performance concrete. *Journal of Sustainable Cement-Based Materials*, 8 (2), 97–143.

Naaman, A., and Hammoud, H., 1998. Fatigue characteristics of high performance fiber-reinforced concrete. *Cement and Concrete Composites*, 20 (5), 353–363.

Nazar, S., et al., 2020. Rheological properties of cementitious composites with and without nano-materials: a comprehensive review. *Journal of Cleaner Production*, 272, 122701.

Omran, A.F., Naji, S., and Khayat, K.H., 2011. Portable vane test to assess structural buildup at rest of self-consolidating concrete. *ACI Materials Journal*, 108 (6), 628–637.

Pilar, R., et al., 2021. Rheological behavior of low shrinkage very high strength self-compacting concrete. *Construction and Building Materials*, 286, 122838.

Qian, Y., et al., 2018. Effect of polycarboxylate ether superplasticizer (PCE) on dynamic yield stress, thixotropy and flocculation state of fresh cement pastes in consideration of the Critical Micelle Concentration (CMC). *Cement and Concrete Research*, 107, 75–84.

Raju, R.A., et al., 2020. Effects of concrete flow on the distribution and orientation of fibers and flexural behavior of steel fiber-reinforced self-compacting concrete beams. *Construction and Building Materials*, 262, 119963.

Rincón, O., and Ocampo, M., 2017. Weak rocks disintegration patterns recognition through image analysis. *In*: *2017 fifteenth IAPR international conference on machine vision applications (MVA)*, 338–341.

Rincon, O., Shakoor, A., and Ocampo, M., 2016. Investigating the reliability of H/V spectral ratio and image entropy for quantifying the degree of disintegration of weak rocks. *Engineering Geology*, 207, 115–128.

Roussel, N., 2006. A thixotropy model for fresh fluid concretes: theory, validation and applications. *Cement and Concrete Research*, 36 (10), 1797–1806.

Sanjayan, J., Jayathilakage, R., and Rajeev, P., 2021. Vibration induced active rheology control for 3D concrete printing. *Cement and Concrete Research*, 140, 106293.

Schmidt, M., and Fehling, E., 2005. Ultra-high-performance concrete: research, development and application in Europe. *ACI Special Publication*, 228 (1), 51–78.

Schwartzentruber, L., Le Roy, R., and Cordin, J., 2006. Rheological behaviour of fresh cement pastes formulated from a Self Compacting Concrete (SCC). *Cement and Concrete Research*, 36 (7), 1203–1213.

Shao, Y., et al., 2022. Impact of fiber distribution and cyclic loading on the bond behavior of steel-reinforced UHPC. *Cement and Concrete Composites*, 126, 104338.

Sohail, M.G., et al., 2021. Durability characteristics of high and ultra-high performance concretes. *Journal of Building Engineering*, 33, 101669.

Soliman, N.A., and Tagnit-Hamou, A., 2017. Using particle packing and statistical approach to optimize eco-Efficient ultra-high-performance concrete. *ACI Materials Journal*, 114 (6), 847–859.

Sritharan, S., et al., 2018. First application of UHPC bridge deck overlay in North America. *Transportation Research Record*, 2672 (26), 40–47.

Swamy, R., 1975. Fibre reinforcement of cement and concrete. *Matériaux et Construction*, 8, 235–254.

Wang, R., et al., 2017. Influence of rheological properties of cement mortar on steel fiber distribution in UHPC. *Construction and Building Materials*, 144, 65–73.

Yoo, D.Y., Kim, S.W., and Park, J.J., 2017. Comparative flexural behavior of ultra-high-performance concrete reinforced with hybrid straight steel fibers. *Construction and Building Materials*, 132, 219–229.

Yu, R., Spiesz, P., and Brouwers, H., 2014. Mix design and properties assessment of ultra-high performance fibre reinforced concrete (UHPFRC). *Cement and Concrete Research*, 56, 29–39.

Zhang, Y., et al., 2020. Improvement of flexural and tensile strength of layered-casting UHPC with aligned steel fibers. *Construction and Building Materials*, 251, 118893.

Zhou, B., and Uchida, Y., 2017. Relationship between fiber orientation/distribution and post-cracking behaviour in ultra-high-performance fiber-reinforced concrete (UHPFRC). *Cement and Concrete Composites*, 83, 66–75.

Zhu, B., et al., 2021. 3D concrete printing of permanent formwork for concrete column construction. *Cement and Concrete Composites*, 121, 104039.